



# Application of Thermodynamic Model for Inclusion Control in Steelmaking to Improve the Machinability of Low Carbon Free Cutting Steels

Xiaobing Zhang<sup>1)2)</sup>, Hans Roelofs<sup>3)</sup>, Stephan Lemgen<sup>4)</sup>, Uli Urlau<sup>3)</sup>, S.V.Subramanian<sup>2)</sup>

*1) currently with Technology Centre, Shanghai No.1 Iron & Steel Co., Baosteel, Shanghai 200126, CHINA and formerly at*

*the time of this research with*

*2) Department of Materials Science and Engineering, McMaster University, Hamilton, Ontario L8S 1C7, CANADA*

*3) Research and Development Department, von Moos Stahl AG, 6021 Emmenbrücke, SWITZERLAND*

*4) Production Manager, von Moos Stahl AG, 6021 Emmenbrücke, SWITZERLAND*

Steel Research int. 75 (2004) No. 5, p 314-321

# Application of Thermodynamic Model for Inclusion Control in Steelmaking to Improve the Machinability of Low Carbon Free Cutting Steels

Xiaobing Zhang<sup>1)2)</sup>, Hans Roelofs<sup>3)</sup>, Stephan Lemgen<sup>4)</sup>, Uli Urlau<sup>3)</sup>, S.V.Subramanian<sup>2)</sup>

<sup>1)</sup> currently with Technology Centre, Shanghai No.1 Iron & Steel Co., Baosteel, Shanghai, China and formerly at the time of this research with

<sup>2)</sup> Department of Materials Science and Engineering, McMaster University, Hamilton, Ontario, Canada

<sup>3)</sup> Research and Development Department, von Moos Stahl, Emmenbrücke, Switzerland

<sup>4)</sup> Production Manager, von Moos Stahl, Emmenbrücke, Switzerland .

Oxide inclusions formed during steelmaking processes influence the machinability of steel products. At moderate and high cutting speeds, the tool life is dominated by chemical wear. However this wear can be suppressed by engineering exogenous and indigenous glassy oxide inclusions in steel. The present work demonstrates a method to engineer glassy oxide inclusions in a low carbon free cutting steel applying a new thermodynamic model for deoxidation control of steel based on slag-melt as well as melt-oxide inclusion equilibration. The model is used online in an industrial production line for the controlled production of glassy inclusions. These inclusions are shown to improve machinability by lubricating the tool-chip interface during machining of the steel at high cutting speeds. Using an inclusion engineered work piece, the crater wear of an uncoated P10 tool is significantly improved and the tool life is tripled at cutting speeds in the range between 200 and 400 m/min. The industrial results show that thermodynamic modelling is a powerful tool to produce free cutting steels with consistently good machinability behaviour.

**Keywords:** thermodynamic model, inclusion engineering, free cutting steel, machinability

## Introduction

The dominant mechanism of tool wear changes from physical wear at low cutting speeds to chemical wear at high cutting speeds. At moderate and higher cutting speeds using cemented carbide inserts in CNC machines, chemical tool wear tends to be a significant problem. **Figure 1** shows a SEM picture of tool wear exhibited by a cemented tungsten carbide tool after cutting AISI 12L14 steel for 15 min at a cutting speed of 200 m/min. The observed crater wear is caused by chemical dissolution of the tool material into the chip due to high temperature at the tool-chip interface and high diffusivity paths associated with local shearing resulting from seizure (atomic contact) at the tool-chip interface [1]. The depth profile of crater wear is related to the cutting speed. When increasing the cutting speed, the crater gets deeper and moves closer to the cutting edge of the tool. Once the cutting edge is damaged, the surface quality of the work piece gets worse. Previous investigations show that neither lead nor manganese sulfide inclusions are effective in suppressing crater wear [2]. However, crater wear can be

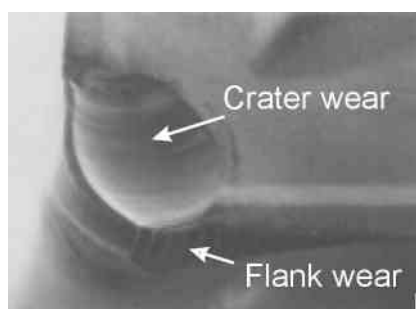


**Figure 1.** SEM picture of WC tool exhibiting pronounced chemical crater wear after cutting AISI 12L14 steel for 15 min at a cutting speed of 200 m/min.

substantially reduced by engineering glassy oxide inclusions in the work piece [3]. The glassy oxide inclusions lubricate the tool-chip interface during machining by forming a viscous layer in-situ at the tool-chip interface. The promotion of sliding tribological conditions by in-situ lubrication at the tool-chip interface suppresses the dissolution crater wear, which is a key to improve the machinability of steels at moderate and higher cutting speeds

In low carbon free cutting steels (LCFCS) the total oxygen content is typically ~100 ppm. At room temperature the oxygen is completely tied up as oxides in deoxidation products which are either hard and crystalline structures or viscous glasses. The behaviour of this very small amount of inclusions during machining is not negligible and varies from causing the harmful effect of abrasive wear to the beneficial effect of lubricating the tool-chip interface [4,5]. Glassy oxide inclusions engineered into steel in steelmaking in-situ form a viscous layer at the tool-chip interface during machining of the steel within a certain temperature range corresponding to a certain cutting speed range. It is the metallurgist's challenge to engineer the best type of oxide inclusions into the work piece steel for self-lubricating the tool-chip interface during machining.

Based on viscosity databases of oxides (at metal cutting temperatures and pressures) the target glassy oxide inclusions to provide sliding tribology at the tool-chip interface can be identified. The goal of the present work was to design a controlled deoxidation process, slag-melt equilibration and melt-oxide inclusion equilibration in steel making to obtain the desirable glassy oxide inclusions. Considering LCFCS similar approaches have been followed focusing on exogenous inclusions (forming in the melt by deoxidation) but ignoring the design of indigenous inclusions (forming during solidification as deoxidation products from the dissolved oxygen) [6,7]. However typically 25–50% of the total oxygen in LCFCS is present as indigenous inclusions. In

comparison to exogenous inclusions the softening point of glassy indigenous inclusions can be considerably lower. Thus if both exogenous and indigenous inclusions are engineered into steels, the range of lubrication is enlarged and extended to lower cutting speeds. In the present work, the target inclusions are of pseudo-wollastonite type (exogenous) and of rhodonite/tephroite type (indigenous).

In order to get the target oxide inclusions during steel making, the residual concentration of strong elements like Al in the melt must be controlled within narrow windows for which slag-metal equilibration is the key. The three essential steps for inclusion control are:

- slag-melt equilibration to control the residual concentration of reactive elements in the melt, such as the soluble aluminium and the soluble oxygen,
- calcium treatment to modify the existing exogenous oxide inclusion in the melt to a target glassy oxide inclusions, and
- the control of the melt chemistry to form indigenous oxide inclusions during solidification of the melt in caster.

Since the control of the target slag composition in the ladle refining furnace (LMF) is dependent upon upstream process control involving minimal carry-over furnace slag and reproducible recovery of deoxidants during primary deoxidation, a clean steel practice is a prerequisite for slag-metal equilibration. In order to perform the above steps under industrial production conditions, a thermodynamic model was developed to predict the exogenous and indigenous oxide inclusions online, and to assist steel makers to control the composition of inclusions within narrow tolerances. A detailed knowledge of elements and compound activities in the molten steel and in the slag is essential for the application of a thermodynamic model to improve the machinability of LCFCS through control the rheology and composition of exogenous and indigenous oxide inclusions during steel making.

This paper outlines a thermodynamic model to evaluate the component activities in a multi-component system based on a sub-regular solution model [8] and its application for control of deoxidation process, slag-melt equilibration and melt-oxide inclusion equilibration to obtain the target glassy oxide inclusions in the melt. The industrial results show that thermodynamic modelling is a powerful tool to produce inclusion engineered steel with consistently good machinability of LCFCS.

### Thermodynamic model

**Chemical reactions.** In this approach, the chemical reactions underlying the deoxidation of the melt, slag-melt equilibration, and

melt-oxide inclusion equilibration are considered. The deoxidation reaction occurring in the melt can be expressed as follows:



where M (M = Al, Si, Mn and Ca) is the dissolved deoxidising element and O is the soluble oxygen in the melt, respectively.  $M_xO_y$  is an oxide product from the reaction (equation (1)), which is in the solid state; x and y are stoichiometric coefficients.

The equilibrium constant of the reaction can be expressed as

$$K_{M-O} = \frac{a_{M_xO_y}}{a_M^x a_O^y} = \exp\left(-\frac{\Delta G_{M-O}^o}{RT}\right) \tag{2}$$

in which,  $\Delta G_{M-O}^o$  is the mole free energy change of the above deoxidation reaction (equation (1)) in the standard state, R is the gas constant, and T is temperature in K.  $a_{M_xO_y}$  is the activity of  $M_xO_y$  in the oxide system referred to pure solid standard state.  $a_M$  and  $a_O$  are the activities of M and O in the melt referenced to 1 weight % solution in iron, respectively.

**Table 1** gives the chemical reactions taking place in deoxidation of the melt, in slag-melt equilibration and in melt-oxide inclusion equilibrium during steel making, and their mole free energy changes in standard state, as well as their reaction constants. The chemical free energy for the deoxidation reactions by silicon, aluminium, calcium and man-

**Table 1.** Thermodynamic data on chemical reactions taking place in deoxidation, slag-metal equilibration, melt-oxide equilibrium.

Chemical reactions	Mole free energy changes $\Delta G_{M-O}^o$ (J/mol)	Constants, $K_{M-O}$ [ $=\exp(-\Delta G_{M-O}^o/RT)$ ]
$\underline{Si} + 2\underline{O} = SiO_2(s)$	$-594230 + 229.73 T$ [7]	$\frac{a_{SiO_2}}{a_{Si} a_O^2}$
$2\underline{Al} + 3\underline{O} = Al_2O_3(s)$	$-1201860 + 323.22 T$ [7]	$\frac{a_{Al_2O_3}}{a_{Al}^2 a_O^3}$
$\underline{Ca} + \underline{O} = CaO(s)$	$-491140 + 146.45 T$ [8]	$\frac{a_{CaO}}{a_{Ca} a_O}$
$\underline{Mn} + \underline{O} = MnO(s)$	$-288120 + 128.26 T$ [7]	$\frac{a_{MnO}}{a_{Mn} a_O}$
$2/3 Al_2O_3(s) + \underline{Si} = SiO_2(s) + 4/3 \underline{Al}$	$207010 - 32.42 T$	$\frac{a_{SiO_2}^{4/3} a_{Al_2O_3}^{2/3}}{a_{Si} a_{Al_2O_3}^{2/3}}$
$SiO_2(s) + 2\underline{Ca} = 2CaO(s) + \underline{Si}$	$388050 - 63.17 T$	$\frac{a_{Si} a_{CaO}^2}{a_{Ca}^2 a_{SiO_2}}$
$SiO_2(s) + 2\underline{Mn} = 2MnO(s) + \underline{Si}$	$-17990 + 26.79 T$	$\frac{a_{Si} a_{MnO}^2}{a_{Mn}^2 a_{SiO_2}}$

ganese in the melt are summarised respectively in table 1. Though silicon deoxidation is the most important one for producing glassy oxide inclusions in LCFCS steel making, the competing reactions in the presence of aluminium, calcium and manganese in the melt are included in the table. The products of deoxidation reactions are complex, involving a multi-component oxide system. Therefore, the data of component activities in the melt as well as in oxide systems are necessary for the calculation of the reactions in LMF.

**Calculation of Activities.** The thermodynamic model calculates element and component activities, respectively in melt and in oxide system, due to the chemical reactions in LMF taking into account Ca, Al, Si, Mn and O.

In the melt the activity of element *i* in steel can be calculated as

$$a_i = f_i[\%i] \tag{3}$$

where [%*i*] is the weight percent of dissolved element *i* in the melt. *f<sub>i</sub>* is the activity coefficient of *i*, which is calculated by the interaction coefficient method as given below:

$$\log f_i = \sum_{j=2}^n e_i^j [\%j] + \sum_{j=2}^n r_i^j [\%j]^2 + \sum_{j=2}^n \sum_{\substack{k=2 \\ j < k}}^n r_i^{j,k} [\%j][\%k] \tag{4}$$

here *e<sub>i</sub><sup>j</sup>* and *r<sub>i</sub><sup>j</sup>* denote the first and the second order interaction parameters respectively [9].

The activity of *M<sub>x</sub>O<sub>y</sub>* in oxide systems can be calculated as

$$a_{M_xO_y} = X_{M_xO_y} \exp\left(\frac{G_{M_xO_y}^{ex} - G_{M_xO_y}^o}{RT}\right) \tag{5}$$

where *X<sub>M<sub>x</sub>O<sub>y</sub></sub>* is the mole fraction of an oxide *M<sub>x</sub>O<sub>y</sub>* in the oxide system, *G<sub>M<sub>x</sub>O<sub>y</sub></sub>*<sup>ex</sup> is the excess partial mole free energy of the oxide in reference to the pure liquid state and *G<sub>M<sub>x</sub>O<sub>y</sub></sub>*<sup>o</sup> is the mole free energy of phase transformation of the oxide from liquid to solid [10]. *G<sub>M<sub>x</sub>O<sub>y</sub></sub>*<sup>ex</sup> is calculated with a sub-regular solution model shown below [8,11].

The excess partial mole free energy *G<sub>M<sub>x</sub>O<sub>y</sub></sub>*<sup>ex</sup> (*M<sub>x</sub>O<sub>y</sub>*=1 to 4) can be expressed with a set of formulae in a multi component system, in which 1 to 4 denote four oxide compounds in a quaternary oxide system respectively.

$$G_1^{ex} = \sum_2^{j'} \sum_0^{k'} \sum_0^{l'} A_{jkl} Y^j Z^k U^l \tag{6-1}$$

$$G_2^{ex} = - \sum_2^{j'} A_{j00} / (1 - j) + \sum_2^{j'} \sum_0^{k'} \sum_0^{l'} \left\{ A_{jkl} Y^j Z^k U^l \left\{ 1 + (j - k) / [Y(1 - j)] \right\} + (k - l) / [YZ(1 - j)] + l / [YZU(1 - j)] \right\} \tag{6-2}$$

$$G_3^{ex} = - \sum_2 \sum_0 A_{jk0} / (1 - j) + \sum_2 \sum_0 \sum_0 \left\{ A_{jkl} Y^j Z^k U^l \left\{ 1 + (j - k) / [Y(1 - j)] + (k - l) / [YZ(1 - j)] \right\} \right\} \tag{6-3}$$

$$G_4^{ex} = - \sum_2^{j'} \sum_0^{k'} \sum_0^{l'} A_{jkl} / (1 - j) + \sum_2^{j'} \sum_0^{k'} \sum_0^{l'} \left\{ A_{jkl} Y^j Z^k U^l \left\{ 1 + (j - k) / [Y(1 - j)] + (k - l) / [YZ(1 - j)] + l / [YZU(1 - j)] \right\} \right\} \tag{6-4}$$

in which *j'*, *k'* and *l'* are the order (four in the present application) of the sub-regular solution model. *Y*, *Z* and *U* are the variables of the molar fractions. Their definitions are *Y*=1-*X<sub>1</sub>*, *Z*=1-(*X<sub>2</sub>*/*Y*) and *U*=1-(*X<sub>3</sub>*/*YZ*). A set of *A<sub>jkl</sub>* parameters in the above equations can be evaluated based on the known boundary conditions. Once *A<sub>jkl</sub>* parameters of an oxide system are evaluated, the oxide activities in the oxide system can be calculated with equation (6-1) to (6-4) and equation (5). **Table 2** gives an overview of all symbols used.

**Figure 2** shows the calculated iso-activities of MnO, Al<sub>2</sub>O<sub>3</sub> and SiO<sub>2</sub> in the MnO-Al<sub>2</sub>O<sub>3</sub>-SiO<sub>2</sub> system at 1500 °C. The *indigenous oxide inclusions* formed during the solidification in carbon steels pertain to the MnO-Al<sub>2</sub>O<sub>3</sub>-SiO<sub>2</sub> system. Thus the oxide activities of the MnO-Al<sub>2</sub>O<sub>3</sub>-SiO<sub>2</sub> system turn out to be the key database for thermodynamic modelling of melt-oxide inclusion equilibration to predict those indigenous oxide inclusions.

The calculated iso-activities of the CaO, Al<sub>2</sub>O<sub>3</sub> and SiO<sub>2</sub> in the CaO-Al<sub>2</sub>O<sub>3</sub>-SiO<sub>2</sub> system at 1600 °C are given in **figure 3**. The *exogenous oxide inclusions* produced by calcium treatment are typical oxide inclusions in this system. The oxide activities of the CaO-Al<sub>2</sub>O<sub>3</sub>-SiO<sub>2</sub> system are

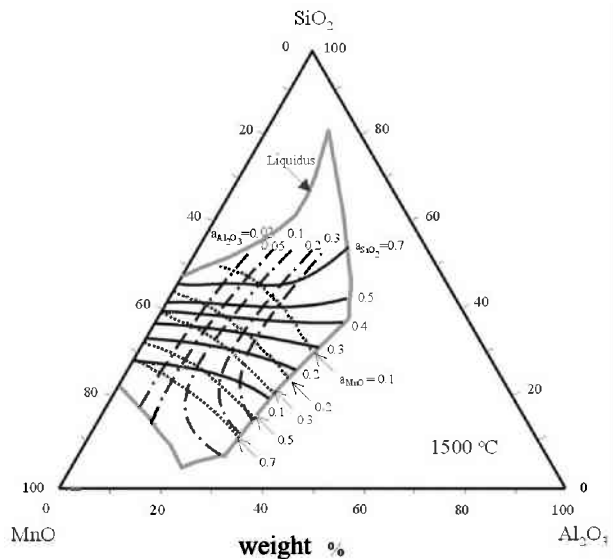


**Figure.2.** Calculated iso-activities of MnO, Al<sub>2</sub>O<sub>3</sub> and SiO<sub>2</sub> in the MnO-Al<sub>2</sub>O<sub>3</sub>-SiO<sub>2</sub> system at 1500°C.

Table 2. List of symbols

Symbol	Explanation
$K_{M-O}$	The equilibrium constant of the reaction $xM + yO = M_xO_y(s)$
$\Delta G_{M-O}^o$	The mole free energy change of the reaction $xM + yO = M_xO_y(s)$
$R$	The gas constant
$a_{M_xO_y}$	An activity of $M_xO_y$ in the oxide system referred to pure solid standard state
$a_M \ a_O$	Activities of M and O in the melt referenced to 1 weight % solution in iron
$f_i$	An activity coefficient of dissolved element $i$
$e_i^j$	The first order interaction parameter of element $i$ with element $j$
$r_i^j$	The second order interaction parameter of element $i$ with element $j$
$X_{M_xO_y}$	A mole fraction of an oxide $M_xO_y$ in the oxide system
$G_{M_xO_y}^{ex}$	An excess partial mole free energy of the oxide in reference to the pure liquid state
$G_{M_xO_y}^o$	A mole free energy of phase transformation of the oxide from liquid to solid
$Y, Z \text{ and } U$	Molar fractions in a quaternary oxide system
$A_{jkl}$	Coefficients in the series expansion (equation 6)

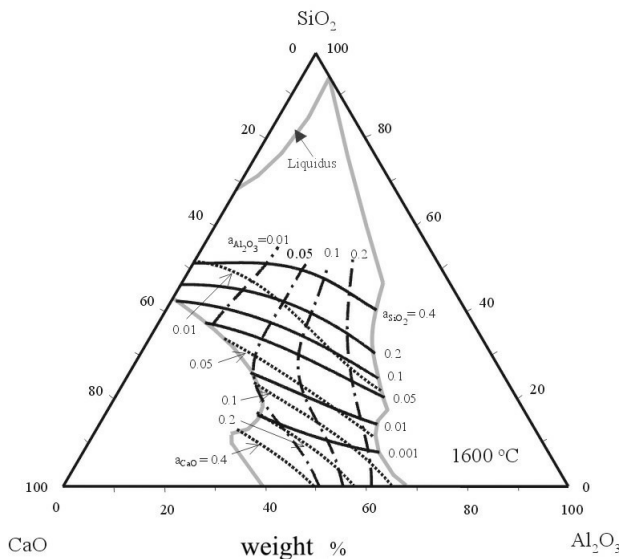


Figure.3. Calculated iso-activities of CaO, Al<sub>2</sub>O<sub>3</sub> and SiO<sub>2</sub> in the CaO-Al<sub>2</sub>O<sub>3</sub>-SiO<sub>2</sub> system at 1600°C.

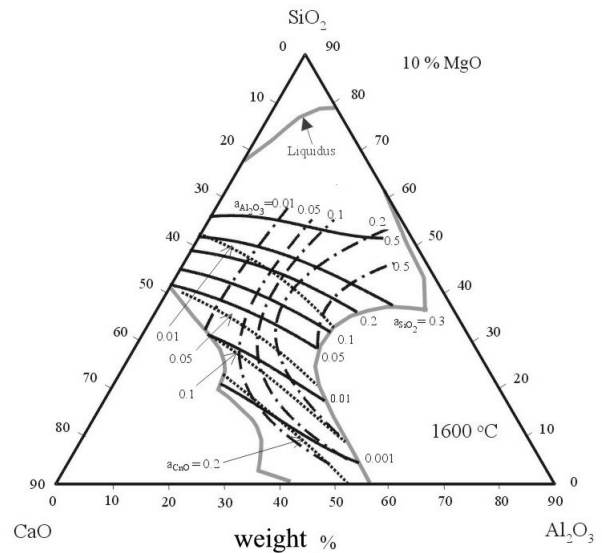


Figure.4. Calculated iso-activities of CaO, Al<sub>2</sub>O<sub>3</sub> and SiO<sub>2</sub> in the CaO-MgO(10wt%)-Al<sub>2</sub>O<sub>3</sub>-SiO<sub>2</sub> system at 1600°C.

hence required for the prediction of exogenous oxide inclusions produced by calcium treatment in LMF.

The *slag composition in LMF* can be represented by the CaO-MgO-Al<sub>2</sub>O<sub>3</sub>-SiO<sub>2</sub> quaternary system for slag-melt equilibration in LMF. Hence, oxide activities are an important database for the design and control of the slag-melt equilibration in LMF in order to achieve the target soluble

concentrations in the melt. **Figure 4** shows the calculated iso-activities of the CaO, Al<sub>2</sub>O<sub>3</sub> and SiO<sub>2</sub> in the CaO-MgO(10wt%)-Al<sub>2</sub>O<sub>3</sub>-SiO<sub>2</sub> system at 1600 °C. By controlling the component oxide activities in the slag in equilibration with the melt, the concentrations of the reactive elements in the melt are controlled to produce exogenous and indigenous oxide inclusions of the required rheology.

The model has been validated in off-line applications by previous industrial studies on slag-melt equilibration, exogenous oxide inclusion and indigenous oxide inclusions [8]. In the present investigation the model was used for deoxidation control of the melt in the LMF station of the von Moos Stahl steel shop. In silicon deoxidation for LCFCS, the resulting oxygen activity now could either be calculated by the model assuming slag metal equilibrium at 1600°C or measured by using CELOX probes. **Figure 5** shows the very first results of four heats differing slightly in chemical composition of the melt and of the LMF slag. The circles represent the measured data which fall on the curves predicted by the model. The close agreement between the model prediction and the actual measurement serves as validation of the model. It can be seen that the effect of increasing silicon content is to decrease the oxygen activity in the melt, which saturates out at large silicon content. However, deoxidation potential of silicon increases with change of slag composition. Decreasing the silica activity of slag decreases the soluble oxygen content in the melt for a given silicon content in accordance with model predictions.

### Inclusion engineering of steel grade 11SMn37

The production line of the steel shop at von Moos Stahl AG is shown schematically in **Figure 6**. In the electric arc furnace (EAF) the scrap is melted and subsequently tapped into the ladle. At this moment primary deoxidation processes are started. Synthetic slag addition, the carry-over slag from EAF and deoxidation products determine the slag composition which has to be controlled within narrow tolerances. At the ladle metal furnace (LMF) small slag corrections can still be done. Slag-metal equilibration is used to control the residual concentration of reactive elements

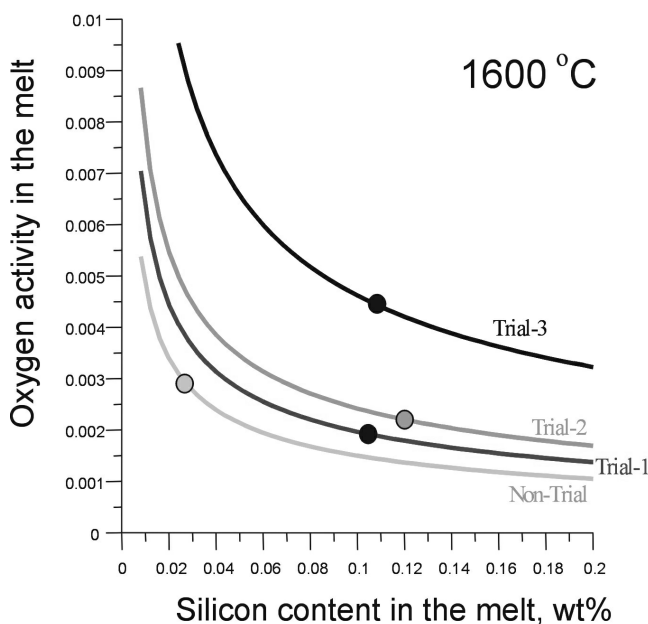


**Figure 5.** Comparison of the oxygen activities measured in the melt and the data calculated by the model under the slag-melt equilibration in LMF at 1600°C.

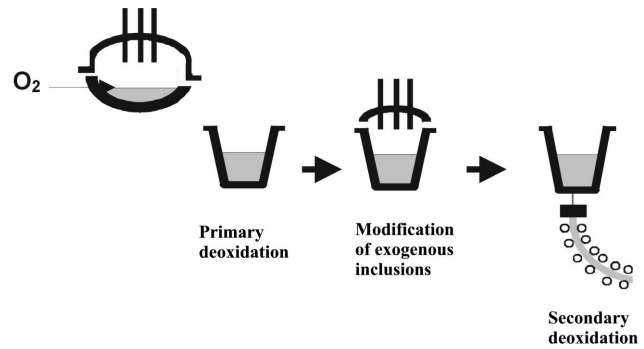


**Figure 6.** Schematic diagram of production line of the steel shop at von Moos Stahl AG.

and soluble oxygen in the melt. Existing exogenous inclusions are modified by Ca treatment. After LMF treatment at 1600°C still 25 – 50 ppm oxygen are dissolved in the melt. Controlled by the chemical composition of the melt, the oxygen forms indigenous inclusions during solidification at the continuous caster. In the standard 11SMn37 grade these inclusions are rich either in Al<sub>2</sub>O<sub>3</sub> or MnO depending on the Al level in the steel and in all cases they are crystalline. To get the beneficial glassy inclusions the silicon content of the steel must be about 0.2 % and the target ratio of CaO/SiO<sub>2</sub> in the LMF slag is close to unity.

The thermodynamic modelling is applied online to predict the compositions of exogenous and indigenous inclusions. This allows for the course correction to achieve the target slag at the LMF station and guarantees a stable process. The three important steps in inclusion engineering of steel for producing glassy oxide inclusions are shown in **Figure 7**. Step-1 is the design of LMF slag to control residual aluminium and residual oxygen contents in the melt through slag-melt interaction (supposing slag-melt equilibrium). The thermodynamic modelling gives the required slag composition. Step-2 is the design of deoxidation processes at the LMF to produce the target glassy exogenous oxide inclusions. A calcium treatment is used to modify existing oxide inclusions in LMF. The expected inclusions are predicted by the model. Step-3 is the design of deoxidation during solidification to form the optimum target indigenous glassy oxide inclusions. The model calculates the inclusion composition for a given melt chemistry.

### Results

Four 80 ton heats of an inclusion engineered 11SMn37 were produced by casting 135 x 135 mm<sup>2</sup> billets and subsequent rolling to wire rods of 33 and 37 mm diameter. At Steeltec, a sister company of von Moos Stahl, the wire rods were cold drawn to 31 and 35 mm bright bars respectively.

**Inclusion characterization.** To verify the inclusion composition SEM/EDX techniques were applied on one inclusion engineered heat using the PSEM of the company RJL Micro & Analytic[12]. By this method a 150.87 mm<sup>2</sup> area section was scanned with a 0.895 μm grid size. The morphology and the chemical composition of every registered

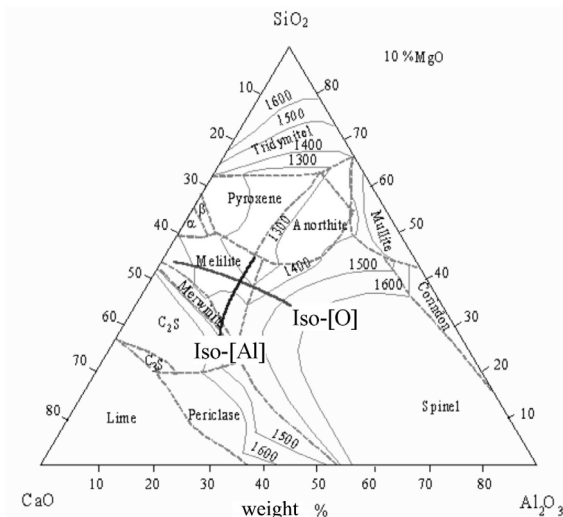


**Figure 7.** Step 1: Design of LMF slag: Prediction of optimum slag composition (based on slag-melt equilibration) to control the demanded soluble Al and O of the melt in LMF.

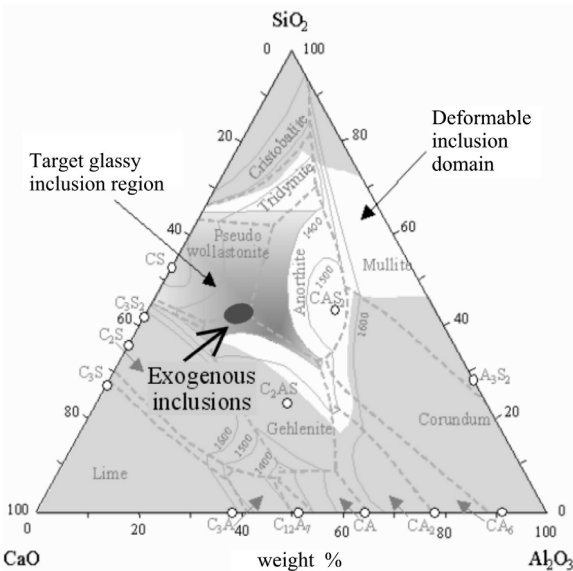


**Figure 7.** Step 2: Design of deoxidation in LMF: Prediction of exogenous inclusions after Ca treatment (based on slag-metal equilibrium).

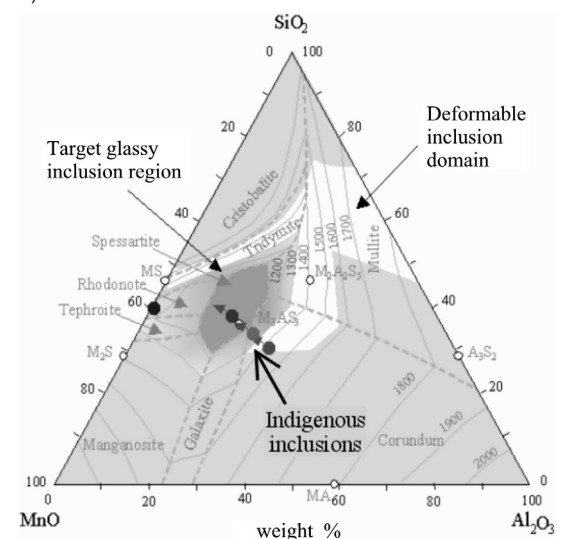


**Figure 7.** Step 3: Design of deoxidation in the continuous caster: Prediction of indigenous inclusions (based on the melt chemistry and thermodynamic equilibrium) after solidification in the caster.

inclusion were analysed. Because of their high amount, sulphides have been filtered out by adequate trigger levels of the reflected signals. Neglecting all measurements with Fe>40% (too much matrix) and with S>10% (dominant sulphide content) 174 particles were detected. From them 158 could be identified either as CaO-Al<sub>2</sub>O<sub>3</sub>-SiO<sub>2</sub>-type (exogenous) or MnO-Al<sub>2</sub>O<sub>3</sub>-SiO<sub>2</sub>-type (indigenous). **Figure 8 and 9** show the compositions of the measured inclusions in the corresponding ternary diagrams. Their chemical compositions are in good agreement with the thermodynamic prediction (assuming thermodynamic equilibrium). The inclusions are located in the dark areas of the target glassy inclusion regions.

**Machinability tests.** The machinability tests (single point turning ) were performed in case of the flank wear

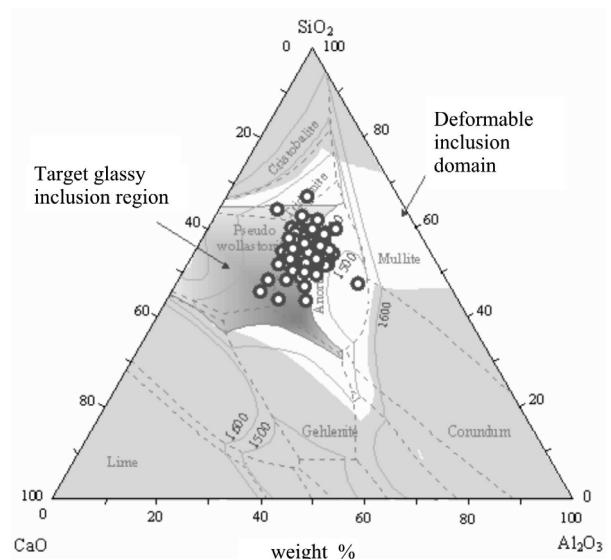


**Figure 8.** EDX analysis of exogenous oxide inclusions of CaO-Al<sub>2</sub>O<sub>3</sub>-SiO<sub>2</sub> in inclusion engineered 11SMn37steel (as rolled).

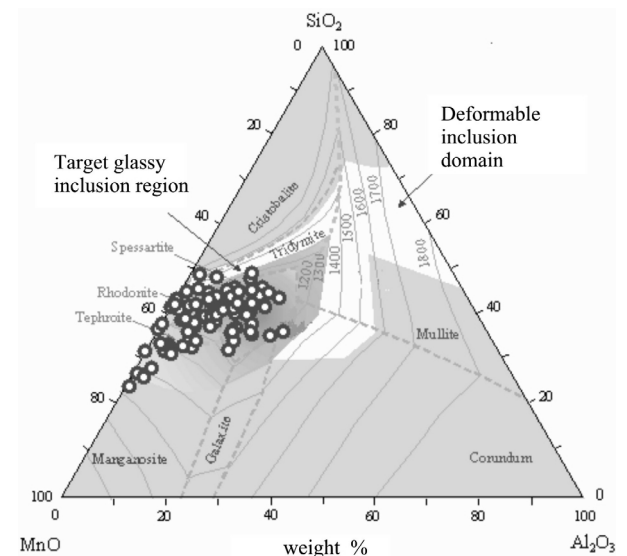


**Figure 9.** EDX analysis of indigenous oxide inclusions of MnO-Al<sub>2</sub>O<sub>3</sub>-SiO<sub>2</sub> in inclusion engineered 11SMn37steel (as rolled).

measurements at the IFW (University of Hannover) and in case of the crater wear characterization at the IWF (ETH in Zürich). To determine the tool life of an uncoated P10 tool under dry conditions, the turning was done at fixed depth of cut (1 mm) and feed rate (0.1 mm/rev) whereas the machining speed was varied from 100 to 400 m/min. The flank wear was measured under an optical microscope. The tool life was measured as the cutting time to reach 0.3 mm flank wear.

The machining performances of four regularly produced 11SMnPb37 were compared with the results of four inclusion engineered heats. **Figure 10** shows the comparison of the tool life of cutting inclusion engineered 11SMn37 and regular 11SMnPb37. Using an inclusion engineered work piece the tool life could at least be tripled at 200 m/min and higher cutting speeds. At 100 m/min no significant difference between the two steel grades were found. At this speed the temperature at the tool edge is not high enough to soften the oxide inclusions.

At higher cutting speeds friction is more pronounced at the rake face of the tool than at the clearance face. This should cause a large temperature rise on the tool rake face promoting crater wear of tools. At increasing cutting speeds crater wear becomes more important than flank wear. Unfortunately the depth and geometry of the crater cannot easily be measured. Also the position of the crater in relation to the tool edge differs considerably with different steel grades. Lead addition diminishes the chip tool contact length resulting in a crater position close to the tool edge whereas the machining of non-leaded steel leads to a more elongated crater that has its maximum depth farther away from the tool edge.

Using an optical laser system the crater profile was analysed by performing line scans perpendicular to the cutting edge. The tools were mounted on a fixed sample holder to guarantee the right (comparable) position of the line scan. The result is shown in **figure 11**. The maximum depth of the crater profile of 11SMnPb37 is twice that of the inclusion engineered steel. It can be clearly seen that in case

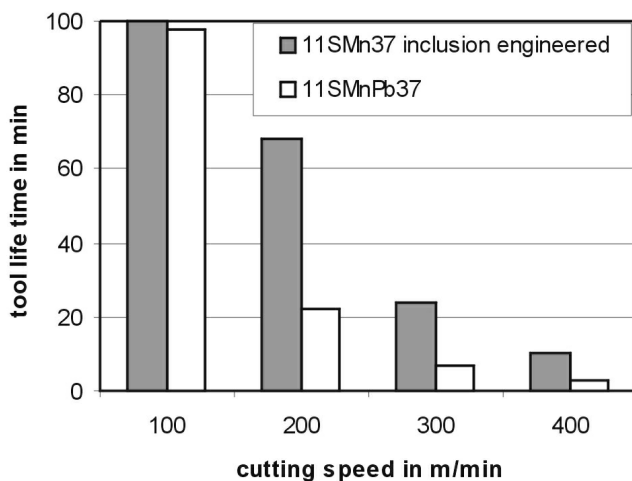


**Figure 10.** The comparison of the tool life of cutting inclusion engineered 11SMn37 and regular 11SMnPb37. Cutting conditions: feed rate = 0.1 mm/rev, depth of cut = 1 mm, uncoated P10 tool, dry machining.

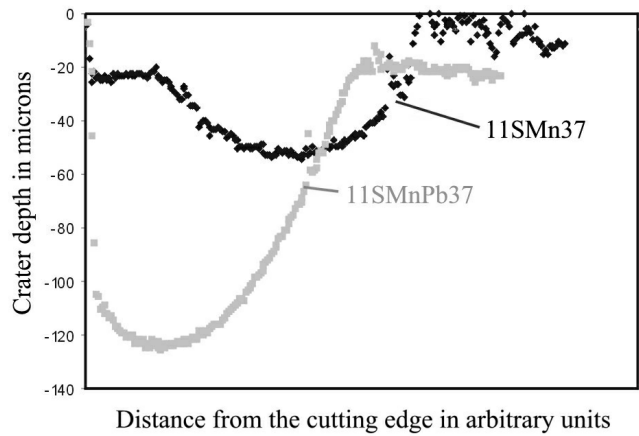


**Figure 11.** Comparison of crater profiles of inclusion engineered 11SMn37 and regular 11SMnPb37 after 4.1 km machining. Cutting conditions: speed = 300 m/min, feed rate = 0.3 mm/rev, depth of cut = 2 mm, uncoated P10 tool, dry machining.

of the leaded steel grade the crater wear is very pronounced at the vicinity of the cutting edge. This is the well known characteristic feature observed in machining leaded steel grades.

### Conclusions

- A thermodynamic model was developed based on the sub-regular solution of multi-component oxide systems applicable for slag-metal equilibrium.
- The model is used as an online tool at the ladle furnace of the von Moos Stahl steel shop for controlling deoxidation processes, slag-melt equilibration and melt-oxide inclusion equilibration. This allows the controlled production of exogenous and indigenous oxide inclusions in accordance with model prediction.
- The controlled production of glassy oxides with adequate viscosity at the tool-chip interface temperature can be used to improve the machinability of low carbon free cutting steels significantly. Using an inclusion engineered work piece the tool life time of an uncoated P10 tool could be tripled at cutting speeds in the range between 200 and 400 m/min.

### Acknowledgements

The authors wish to acknowledge the contributions of Chr. Hollmann of IFW (University of Hannover) for flank wear results and helpful discussion, M.Cobet of IWF (ETH Zürich) for crater wear measurements, and B. Heneka of RJL Micro&Analytic GmbH for oxide inclusion characterization applying SEM/EDX techniques. The steel making trials were performed with the help of M. Kühnemund and W. Fuchs of von Moos Stahl.

The funding support for the basic science research by NSERC, Canada is gratefully acknowledged in the form of a grant to R. Sowerby.

(A2004005; received on 2 December 2003, in final form on 11 February 2004)

Contact: Dr. sc. nat. Hans Roelofs  
 Von Moos Stahl AG  
 Postfach 2044  
 6021 Emmenbrücke / Switzerland

## References

- [1] S.V. Subramanian, D.A.R. Kay: "Microstructural Engineering for Enhanced Machinability", Proc. 38th MWSP conf. ISS, 34 (1997), 125/35.
- [2] K. Ramanujachar and S.V. Subramanian: *Wear*, 197 (1996), 45/55.
- [3] S.V. Subramanian and K. Ramanujachar: "Strategies to Replace Lead in Free-Cutting Steels", Proc. 37th MWSP conf. ISS, 33 (1996), p. 341-353.
- [4] S.V. Subramanian, H.O. Gekonde, X. Zhang, J. Gao: *Ironmaking and Steelmaking*, 26 (1999), 333-338.
- [5] S.V. Subramanian, X. Zhang, U. Urlaub, H. Roelofs: "Design of Inclusion Engineered Steel for High Speed Machining", 4th Int. Conference on Metal Cutting and High Speed Machining, Darmstadt, March 19-21, 2003.
- [6] C. Bertrand and D. Maza: "Optimizacion de los Aceros para Mecanizados a Alta Velocidad de Corte", EUR18009, 1998.
- [7] G. Pierson and B. Sander: "Amélioration des Performances de Coupe des Aciers Doux de Décolletage par Maitrise de leur Contenu Inclusif", EUR16020, 1995.
- [8] X. Zhang and S.V. Subramanian: "Thermodynamic Modelling for De-oxidation Control of Steel in LMF", Proc. of the 85th Steelmaking Conference, Nashville, Tenn., U.S.A., March 10-13, 2002, pp. 313-322.
- [9] *Steelmaking Data Sourcebook*, The Japan Society for the Promotion of Science, The 19th Committee on Steelmaking, Gordon and Breach Science Publishers, New York, NY, 1988, p.280/97.
- [10] S. Ban-Ya and M. Hino, "Thermochemical Properties of Selected Oxides and Slags", *Chemical Properties of Molten Slags*, The Iron and Steel Institute of Japan, 1991, p.1-22.
- [11] X. Zhang, G. Jiang, K. Tang, W. Ding and D. Xu: *Calphad*, 21 (1997), No 3, 301/9.
- [12] "Analyse nichtmetallischer Einschlüsse im Stahl", in-house publication 8/2003 RJL Micro & Analytic GmbH, Karlsdorf-Neuthard, Germany.